



# Cryo-printed microfluidics enable rapid prototyping for optical-cell analysis

Rokas Garmasukis<sup>1,2</sup> · Claudia Hackl<sup>1</sup> · Christian Dusny<sup>2</sup> · Christian Elsner<sup>1</sup> · Ales Charvat<sup>1</sup> · Andreas Schmid<sup>2</sup> · Bernd Abel<sup>1,3</sup>

Received: 17 February 2022 / Accepted: 10 November 2022 / Published online: 25 November 2022  
© The Author(s) 2022

## Abstract

This paper highlights an innovative, low-cost rapid-prototyping method for generating microfluidic chips with extraordinary short fabrication times of only a few minutes. Microchannels and inlet/outlet ports are created by controlled deposition of aqueous microdroplets on a cooled surface resulting in printed ice microstructures, which are in turn coated with a UV-curable acrylic cover layer. Thawing leaves an inverse imprint as a microchannel structure. For an exemplary case, we applied this technology for creating a microfluidic chip for cell-customized optical-cell analysis. The chip design includes containers for cell cultivation and analysis. Container shape, length, position, and angle relative to the main channel were iteratively optimized to cultivate and analyze different cell types. With the chip, we performed physiological analyses of morphologically distinct prokaryotic *Corynebacterium glutamicum* DM1919, eukaryotic *Hansenula polymorpha* RB11 MOX-GFP, and phototrophic *Synechocystis* sp. PCC 6803 cells via quantitative time-lapse fluorescence microscopy. The technology is not limited to rapid prototyping of complex biocompatible microfluidics. Further exploration may include printing with different materials other than water, printing on other substrates in-situ biofunctionalization, the inclusion of electrodes and many other applications.

**Keywords** Cryo-printing · Ice-printing · Microfluidics · Rapid-prototyping

## 1 Introduction

What is so fascinating about seeing an igloo, an intricate ice sculpture or a snowflake through microscope lens for the first time? One of the reasons may be the idea that something so prevalent in everyday life as water in its liquid state has been used to create something unusual, practical and beautiful in solid one. Indeed, ice is abundant, easy to sculpt and at the same ephemeral. Using its properties of solidity and evanescence, we take ice to the microfluidics field to “sculpt” microfluidics chips.

But why yet another method when there are many other technologies to fabricate microfluidic chips? PDMS-based microfluidics is the most well-known option and has contributed greatly to the growth of this field, due to several key factors inherent to replica-molding techniques—low-cost set-up for fabrication in a university setting, biocompatibility, optical transparency, gas permeability, conformal sealing between PDMS and other surfaces, and elasticity of PDMS (Sackmann et al. 2014). However, even though some properties of PDMS allow for a great variety of microfluidic devices to be created, other properties hinder the adaptation of microfluidic technology to mainstream practice. Leaching of uncrosslinked oligomers of PDMS into solution, as well as absorption of organic solvents, small molecules, proteins and nanoparticles, vapor permeability are named as culprits for that (Chalfie et al. 1994; Cubitt et al. 1995; Dusny et al. 2015; Grünberger et al. 2013). The modifications to PDMS-based chips to avoid these problems often call claimed biocompatibility into question (Sackmann et al. 2014). Another drawback of PDMS soft lithography is the low feasibility for scaling-up, and transfer of results to standard plastic

✉ Christian Dusny  
christian.dusny@ufz.de

<sup>1</sup> Leibniz Institute of Surface Engineering (IOM),  
Permoserstrasse 15, 04318 Leipzig, Germany

<sup>2</sup> Helmholtz-Centre for Environmental Research (UFZ),  
Permoserstrasse 15, 04318 Leipzig, Germany

<sup>3</sup> Ostwald-Institute of Physical and Theoretical Chemistry,  
University Leipzig, Linnestrasse 3, 04103 Leipzig, Germany

materials used for mass production is difficult. Many other microfabrication methods exist, such as silicon micromachining, in situ injection molding, micromolding of thermoplastic polymers, and laser ablation of polymer surfaces (Beebe et al. 2002). While these methods are capable of large-scale production, they often require expensive equipment, are not flexible for design changes, involve many steps, and are prone to error, and time-consuming (Beebe et al. 2002; Ho et al. 2015). Because of these and other reasons, researchers are still exploring alternative options for chip fabrication. Thermoplastics such as polycarbonate (PC), poly(methyl methacrylate) (PMMA), polystyrene (PS), and polysulfone (PSU) coupled with solvent imprinting and bonding provide rapid prototyping technologies with fabrication times from 2 h down to 15 min per design (Jiang et al. 2015; Sun et al. 2007).

Another promising alternative for the fabrication of microfluidic devices is three-dimensional (3D) printing, whose advantages, challenges and recent advances were extensively discussed in several reviews (Amin et al. 2016; Au et al. 2016; Nielsen et al. 2020; Waheed et al. 2016). Designs can be adapted reprinted easily, making 3D-printing suitable for prototyping and testing-based optimization, and implementation of the third dimension allows for highly sophisticated and complex structures. Common 3D printing methods used for creating millifluidic devices are stereolithography (SLA), PolyJet (PJ) and fused deposition modelling (FDM). Regarding small channels (< 100  $\mu\text{m}$ ), digital light processing (DLP)-based SLA is the most promising field so far (Nielsen et al. 2020). Further development in this field focus on improvement of the SLA 3D printers and customized resins for producing channels < 50  $\mu\text{m}$ . New approaches, which allow for high-speed stereolithographic printing, involve continuous liquid interface printing (CLIP) (Tumbleston et al. 2015) and computed axial lithography (CAL) (Kelly et al. 2019), which, in case of CAL, allow for the construction of structures in centimeter-scale in less than one minute.

A rapid and inexpensive approach combining cutting of PET-PVA with a craft cutter and lamination to generate microfluidic chips was reported by Levis et al. (Levis et al. 2019). The chips were prepared within 15 min from design to use and applied in high-resolution imaging of cells and organs as well as multi-layered devices for chemical and mechanical actuation for biomechanical studies. The capabilities of alternative approaches, such as cryo-printing, are still unexplored; until now, ice-printing combined with adhesive sealing was used to create a pre-sealed drug delivery chip, a pre-sealed mixing reactor as well as a microcapsule array for multitarget assay

(Zhang et al. 2014, 2015). Furthermore, the technology was used for the fabrication of glucose detection chips (Zheng et al. 2018). We, improve on this technology by decreasing production time to only a few minutes and coupling it with high-resolution printing to create rapidly designed biocompatible microfluidic chips for cell analysis. Chips with customized designs can be fabricated in less than 10 min featuring channels of approximately 100  $\mu\text{m}$  width, with an ability to specify printing position down to 1  $\mu\text{m}$  on  $x$  and  $y$  axes. With this method, 2D and simple 3D volumetric geometries like wells and ports can be printed, although more complex 3D structures cannot be realized. A fully functioning cryo-printing setup costs approximately 50,000 €, while the materials and chemicals used amount to less than 1\$ per chip. We applied cryo-printing to create customized microfluidic bioreactors for isolating, cultivating, and analyzing microbial cells. Different microfluidic chips were developed and successfully used for cell cultivation and analysis under changing environmental conditions with time-resolved bright-field and fluorescence microscopy. The goal was to create an alternative solution to another in-house created single-cell analysis device such as the “Envirostat” (Dusny and Schmid 2015; Rosenthal et al. 2015), which offers excellent environmental control and convection-only-based mass transfer. Compared to the latter, cryo-printing technology has low costs per chip, offers a much higher degree of structural flexibility and easier handling. Three different types of microbial cells being morphologically and physiologically distinct were cultivated and analyzed, namely prokaryotic amino acid-producing *Corynebacterium glutamicum* DM1919, the eukaryotic yeast *Hansenula polymorpha* RB11 MOX-GFP, and the phototrophic cyanobacterium *Synechocystis* sp. PCC 6803. The chips included a cell chamber per one channel network to catch, cultivate, and analyze approximately 30 single cells in parallel; two of such networks were included on a single chip. It offered both diffusion and convection-based, quick medium exchange, which enabled dynamic experiments. In addition to quantitative growth experiments of *Corynebacterium glutamicum* DM1919, cell-to-cell heterogeneity in protein production capacity could be monitored in individual *H. polymorpha* RB11 MOX-GFP cells. Finally, the ability of a pHluorin-equipped *Synechocystis* sp. PCC 6803 cyanobacterium to report the extracellular pH was tested under dynamic pH conditions. Growth rates and cell physiology in the chips were comparable to shake-flask cultivations of the respective strains and approve the biocompatibility of the produced chips. Our results demonstrate the potential of cryo-printing for the rapid-prototyping of customized microstructured chips for cell-based biomicrofluidics.

## 2 Methods

### 2.1 The cryo-printer

#### 2.1.1 Principle of the cryo-printing approach

The basic principle of the presented cryo-printing technology included a two-step process of aqueous ice-channel printing followed by encapsulation of these channels with acrylate. The ice channels were printed by the deposition of water droplets on a cooled substrate. Upon contact with the cold substrate, ice beads were formed; a string of such partially overlapping beads formed one continuous channel. The inlet and outlet ports of the printed channel structures were made by successive printing of ice beads on top of each other to form a “cylinder” higher than the deposited acrylate cover layer. In the second step, the printed ice structures were covered with a liquid mixture of acrylic monomers and a photoinitiator. Finally, the acrylic mixture was cured using a UV-LED (395 nm), resulting in the desired microfluidic channel structure with integrated inlet and outlet ports after thawing.

#### 2.1.2 Set-up of the cryo-printer

The cryo-printer was installed in a closed box with acrylic glass walls and a top cover (Fig. 1). The substrate on which the channels were printed was clamped onto a thermoelectric module (Quick-Ohm Küpper & Co. GmbH, Wuppertal, Germany) installed on a two-axis motorized linear stage (Newport Corporation, Irvine, USA). Before and during the printing, the box was constantly flushed with nitrogen through two square-shaped copper pipes placed at the top and the bottom of the box to exclude water vapor from it. Residual humidity inside the printer box was constantly monitored by a humidity sensor (B&B Thermo-Technik GmbH, Donaueschingen, Germany) connected to an Arduino controller. The temperature of the Peltier element, whose hot side was cooled with a thermostat chiller (JULABO GmbH, Seelbach, Germany), was controlled via a PID process controller (JUMO DICON 500, JUMO GmbH & Co. KG, Fulda, Germany). The printing was initiated by executing a chosen trajectory file from the personal computer, which controlled both the 50  $\mu\text{m}$  micro-dispenser system (Microdrop Technologies GmbH, Norderstedt, Germany) as well as the motion controller (Newport Corporation) steering the two-axis robotic driver long-travel translation stages. The channels were printed by moving the mounted substrate at the given trajectories under the micro-dispenser head which was turned on and off. The droplet frequency was set by an

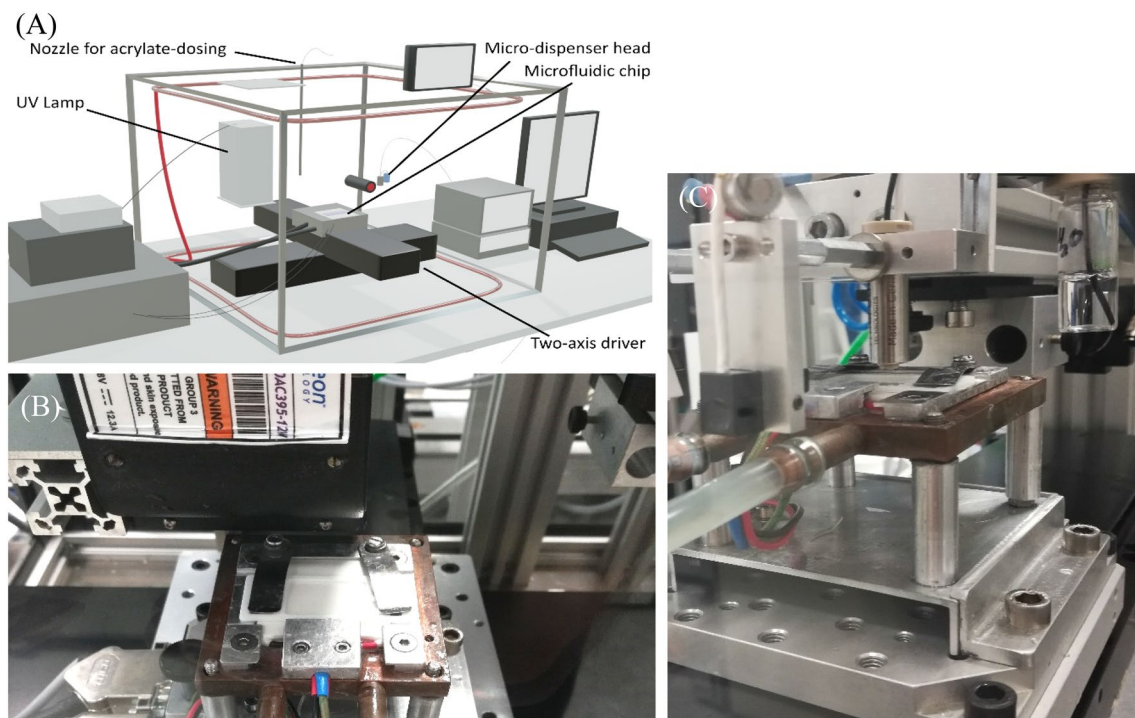


**Fig. 1** Setup of the cryo-printer. **A** Representation of the setup. **B** Microfluidic chip being driven under the UV lamp. **C** Microfluidic chip under micro-dispenser during printing

external digital pulse generator (Stanford Research Systems, Sunnyvale, USA), while the droplets were observed by a high-speed (150 fps) camera (FLIR Systems Inc., Orlando, USA) coupled to the computer. Once the printing was done, the motorized stage moved the substrate under the acrylate-dispenser nozzle, where the acrylic monomer-mixture with photoinitiator was dosed either manually or using a low-pressure syringe pump system to cover the channels with an acrylic layer. The acrylate was polymerized using a 395 nm UV-LED (12 W/cm<sup>2</sup>, Phoseon FireJet™, IGB-tech GmbH, Friedelsheim, Germany).

## 2.2 Microfluidic chip fabrication

### 2.2.1 Cover layer acrylate mixture

As cover layer acrylate, an in-house developed low-viscosity mixture was used, containing 80 wt% monofunctional cycloaliphatic acrylate monomers (Arkema, Düsseldorf, Germany), 15 wt% tetrafunctional polyether acrylate crosslinker (Allnex, Frankfurt am Main, Germany), 5 wt% acidic acrylate adhesion promoter (Allnex) and 3 wt% photoinitiator Omnirad TPO-L (IGM Resins, Waalwijk, Netherlands). Usually, 30 g batches were prepared by weighing the desired amounts of monomers and photoinitiator and mixing them on a vortex shaker. The mixture was left for some time before use, as the adhesion promoter was added in excess, and kept dark in order to prevent polymerization.

Adhesion of the UV-crosslinked acrylate to glass was evaluated on coated glass plates (10 cm × 10 cm, cured acrylate layer thickness 150–230 μm) by incubation in water at room temperature for up to 14 days as well as cross-cut test according to ISO 2409.

Samples for the *in vitro* cytotoxicity test were prepared according to ISO 10993-12 and tested according to ISO 10993-5 using cell line L929 and XTT test (for further details, see SI 1.1).

### 2.2.2 Preparation of coverslips for cryo-printing

As the fabricated microfluidic chips were later used for cell analysis using oil-immersion microscopy, thin 24 × 60 × 0.17 mm glass coverslips (Carl Roth GmbH, Karlsruhe, Germany) were chosen as a chip substrate. Good adhesion of the acrylic layer to the glass surface of the coverslip was crucial to obtain well-performing microchips. For that reason, the glass coverslips were silanized with 3-(trimethoxysilyl)propyl methacrylate (Evonik, Rheinfelden, Germany) before the printing process. First, the coverslips were cleaned in a mixture of 1 M NaOH (Sigma Aldrich, Steinheim, Germany) and 35% H<sub>2</sub>O<sub>2</sub> solution (Merck KGaA, Darmstadt, Germany) (50:50 vol%) for 30 min, washed with distilled water and dried in a compartment drier for 60 min

at 80 °C. They were subsequently silanized by immersion in a microscope slide staining jar filled with a solution of 3-(trimethoxysilyl)propyl methacrylate in ethanol (VWR International, Leuven, Belgium) (5:95 vol%, MEMO: EtOH absolute) for 60 min and dried in a compartment drier overnight at 80 °C.

### 2.2.3 Cryo-printing of the microfluidic chip

A 3D-printed flexible supporting structure was attached to the coverslip (Fig. 2A). It served two functions: (1) to protect the fragile coverslip and (2) to contain the liquid acrylic mixture, which was poured onto the coverslip later in the printing process. Then, the coverslips were clamped onto the thermoelectric module. A thin oil layer between the coverslip and the thermoelectric module was used for more efficient heat dissipation to be able to cool the coverslip quicker and more evenly. After the chip was mounted, the box was flushed with nitrogen until the humidity inside reached 0%. Only then the cooling system was turned on, and the coverslip was cooled down to approximately –30 °C at 100% thermoelectric module cooling capacity (it was essential to reach 0% humidity level before turning on the cooling; otherwise, ice-crystals would have begun to form on the substrate glass). The printing was initiated through the propriety computer software delivered together with the motion controller. The channels were printed by turning the water-droplets producing micro-dispenser nozzle on and off while the *x,y*-motorized stage drove the trajectories (Fig. 2B). The stage coordinates could be specified down to 1 μm. The driver speed was set to 3.75 mm/s, while the droplets were generated at a frequency of 120 Hz. For inlet/outlet holes, hollow cylinder-like structures were created by printing multiple circles on top of each other until the required height was achieved (Fig. 2C). Afterward, the coverslip was moved under the acrylate dispensing nozzle, where approximately 0.3 mL of acrylate mixture with photoinitiator was dispensed manually to cover the area inside the supporting structure (Fig. 2D). Once the acrylic mixture was spread evenly, the cover slide was moved under the UV-LED, where the acrylate was irradiated for 2 s at a wavelength of 395 nm (Fig. 2E). Finally, the cooling was turned off, the ice channels melted at room temperature, resulting in a microfluidic chip with the desired channel network with integrated ports.

Before attaching the port olives, the chip was optionally flushed with attachment factor solution using a disposable tapered curved tip syringe. The stand-alone female olive ports (Microfluidic ChipShop, Jena, Germany) were glued onto the inlets and outlets of the chip by double-sided adhesive tape rings of 1 mm inner diameter (Microfluidic ChipShop), and subsequently, epoxy resin adhesive was placed at the base around the olives to make it leak-proof. After the silanization of the glass surface, the whole fabrication

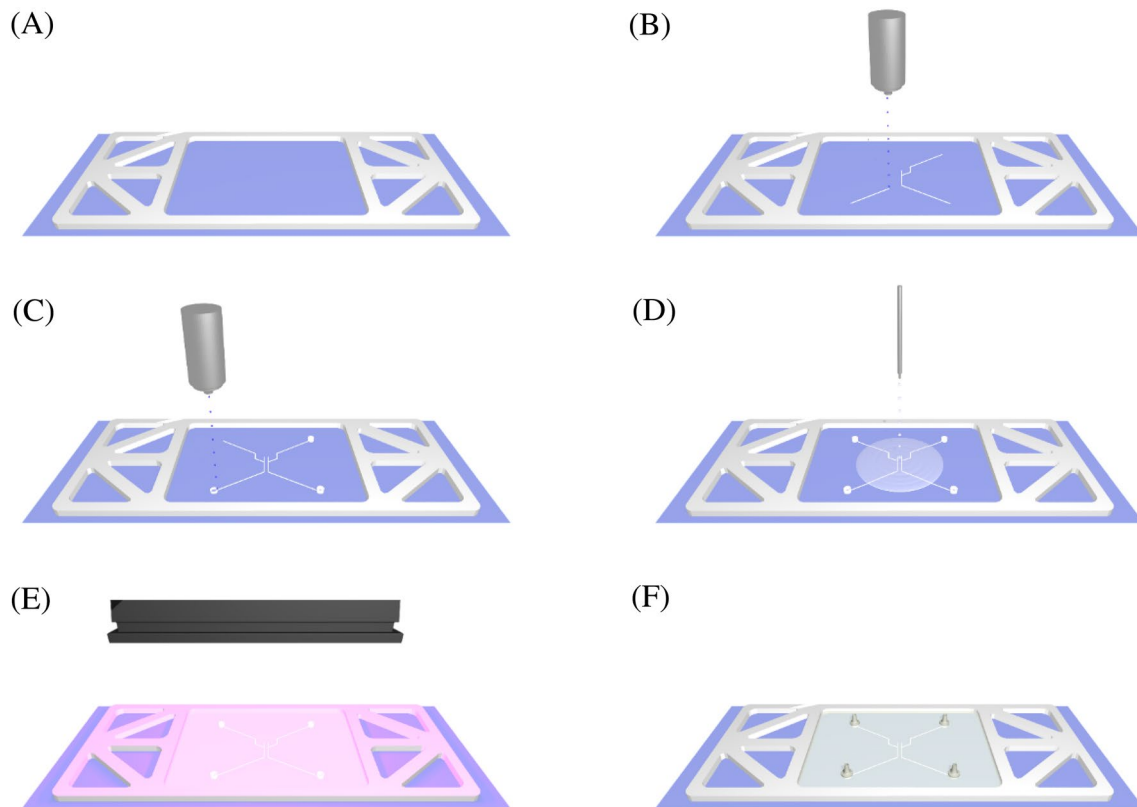


**Fig. 2** Fabrication of a cryo-printed microfluidic chip. **A** Attaching 3D-printed plastic support onto the pretreated cover slip. **B** Printing of ice-channels on the cooled coverslip using the micro-dispenser nozzle. **C** Continuing printing the cylinder-like structures for inlets/

outlets. **D** Covering the printed channels with acrylic mixture. **E** Curing of the acrylic layer with UV-LED. **F** Attaching the olives onto inlets/outlets

process, including the attachment of port olives, took 50 min per chip at maximum for it to be ready to use for experiments, with 40 min needed to glue the olives and for the epoxy adhesive to harden. Alternatively, a customized chip holder with drillings for connectors could be used, cutting down the preparation time of a microfluidic chip to approximately 5 min.

### 2.3 Scanning electron microscopy

To prepare the SEM samples, the microfluidic chips were broken perpendicular to the direction of the channel. The samples were sputter-coated with an approximately 20 nm thin gold layer. The samples were imaged in a high voltage mode of 5 kV using an Ultra-55 SEM (Carl Zeiss Microscopy GmbH, Oberkochen, Germany).

### 2.4 Medium exchange in the cell container

The medium exchange in the cell container of the microfluidic chip was tested by attaching two 10 mL syringes connected to an in-the-chip integrated Y-piece – one with

water and one with 0.1 mM fluorescein solution—to the single inlet of the microfluidic chip. Flow rates of water and fluorescein were varied stepwise between 50 and 250  $\mu\text{L}/\text{h}$  with a neMESYS low-pressure syringe pump system (CETONI GmbH, Korbussen, Germany; see SI 1.2 for specific flow rates) with a switching frequency between them of 2 per hour. The images of the cell container were taken via time-lapse microscopy at 10 s imaging intervals with 100 $\times$  magnification using a 470 nm TL-LED at 25% intensity. The exposure time was 30 ms, binning was set to 1 $\times$ 1 (Zeiss Observer Z1, Carl Zeiss Microscopy GmbH, Jena, Germany). Analysis of fluorescence intensities was carried out via Zeiss Zen Blue (Carl Zeiss Microscopy GmbH, Jena, Germany).

### 2.5 Cell preparation and cultivation

The chip was flushed manually with Millipore water for all experiments until the residual air bubbles in the cell container were dissolved. In the next step, the chip was flushed with 1 mL of the cell-specific medium used in the biological experiments. The cells were deposited by attaching the cell

suspension-containing syringe to the chip and manual flushing (see Sect. 3.1.3). When the cell container was loaded, the chip was attached to the medium-containing syringe, and the remaining cells were flushed out at a flow rate of 3000  $\mu\text{L}/\text{h}$  before lowering it down to the experiment-specific flow rate. For automated pumping of liquids, low-pressure neMESYS syringe pumps were used (Cetoni GmbH, Korbussen, Germany). The microfluidic cultivation experiments were monitored via time-lapse microscopy (Zeiss Observer Z1, Carl Zeiss Microscopy GmbH, Jena, Germany) with 1000 $\times$  total magnification and at an imaging frequency of 30 min. For specific information on cell preparation and cultivation, see SI 1.3.

## 3 Results and discussion

### 3.1 Design of the microfluidic chip

#### 3.1.1 Channel design

A microfluidic cryo-printed chip was designed to enable the cultivation and analysis of various types of microorganisms at the single-cell level. The chip design used for the microfluidic cultivation experiments is shown in Fig. 3. Two independent channel networks were integrated into one microfluidic chip, which allowed for carrying out two independent experiments simultaneously. In principle, the networks can be scaled up to enable at least four independent cultivation experiments per chip. One channel network consisted of an inlet, a cell container, and an outlet. For experiments that required flushing the chip with two or more different liquid media, a different channel design with a printed Y-channel junction and two inlets per channel system or an external Y-piece adapter was used. Both SEM scans and microscopy bright-field images showed the channel width to be between 100 and 160  $\mu\text{m}$  (Fig. 3C–E), resulting from different microdispenser settings for droplet generation during the printing. The height of the channels was approximately 60  $\mu\text{m}$  (Fig. 3E–F). While the size of the micro-dispenser nozzle is the determining factor in respect to the size of the channel, a more detailed study of different settings is yet to be carried out. At the point of junctures, where two channels overlapped, the total height was higher (Fig. 3D). The channel surface displayed characteristic ripples due to the nature of the printing process in which channels are created by frozen water droplets overlapping over each other (Fig. 3C, D, F). While it would have been possible to mitigate the creation of ripples to some extent by choosing different printing settings, it was printed in the present form with the intention to help to avoid cells sticking to the channel walls. They had no measurable effect on the character of the flow.

#### 3.1.2 Cover layer acrylate

The composition of the acrylate mixture serving as cover layer in the cryo-printing process was extensively optimized to gain functioning microfluidic chips on the one hand, and, making it even more challenging, chips that are suited for performing optical cell experiments at single-cell resolution on the other hand.

Viscosity of the acrylate precursor mixture was kept low to enable covering of the printed structures in a reasonable time and, more particularly, under cooling at  $-30\text{ }^{\circ}\text{C}$ . This was achieved by using low viscous monomers as main compounds, e.g., isobornyl acrylate, which also provided excellent adhesion properties. Viscosity of the acrylate mixture was determined to be 3.8 mPa·s (shear rate 1000/s, 25  $^{\circ}\text{C}$ ). Double bond conversion was optimized in order to reduce toxic effects by leaching and ranged from 96 to 100% (ATR-IR, measured on both sides of the acrylate layer). Proper adhesion of the cover layer to the glass substrate was crucial to obtain functioning microchips, therefore, adhesion was evaluated on coated glass plates by incubation in water at room temperature as well as cross-cut test. It was found, that a prior silanization of the glass substrate was necessary to obtain a covalent acrylate-to-glass bonding. Without silanization, all tested acrylate mixtures detached from glass during storage in water within few minutes to hours, while it remained stable for at least 14 days when silanized glass was used. This was also confirmed by SEM images taken from the cross-sections of printed microfluidic chips: prior silanization of the glass led to good bonding at the interface between glass and acrylate layer (Fig. 3E), while delamination occurred at the edges of the channel without silanization. The cross-cut test showed a significant improvement as well: classification 5 without vs. classification 1 with prior silanization. Regarding optical properties, a high optical transmittance and a low autofluorescence of the material in the visible range of light was essential. Transmittance was determined to be in the range of 85–91% for wavelengths between 420 and 800 nm. This is slightly lower compared to elastomeric PDMS-based microfluidics, which are highly optical transparent over the near UV–Vis with a transmittance of  $>90\%$  (Reidy et al. 2019; Stankova et al. 2016). Microfluidic devices fabricated from thermoplastic polymer materials, e.g. PMMA, PC, PS, COC and COP, show comparable transmittance values in the visible range (microfluidic ChipShop). Regarding 3D-printed microfluidic devices, reported transmittances are significantly lower, namely in the range of 60% (Morgan et al. 2016; Shallan et al. 2014). Fluorescence microscopy was performed at excitation wavelengths of 410 nm and 488 nm. Autofluorescence of the cured acrylate layer was negligible for excitation at 488 nm and slightly increased for

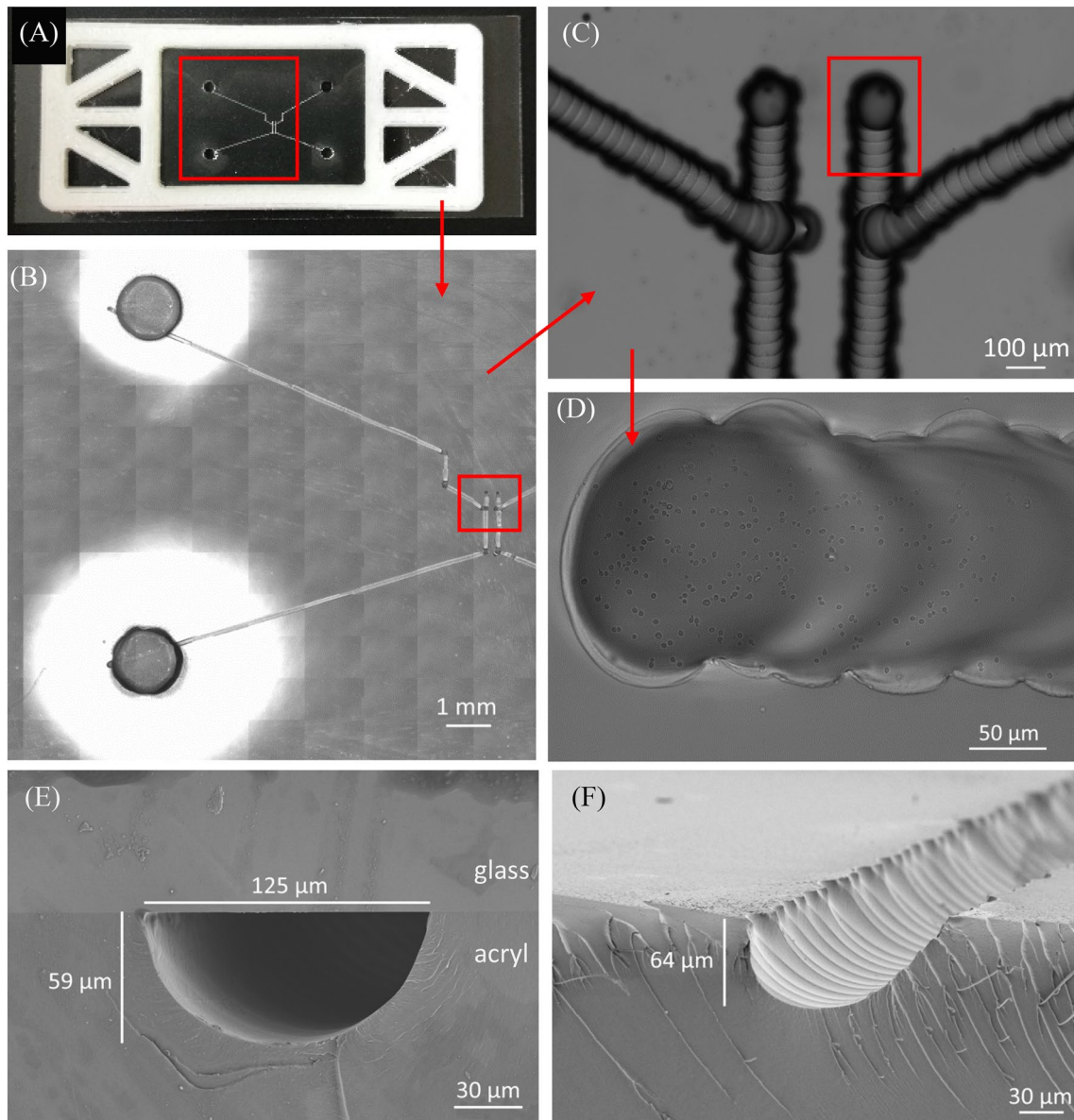


**Fig. 3** Cryo-printed microfluidic chip as used in the experiments discussed in this paper. **A** A photograph of the chip. Red area is represented by image **(B)**. **B** Bright-field image of two cell containers in the middle, one inlet in the bottom and one outlet at the top. Red area is represented by image **(C)**. **C** Bright-field image of two cell containers, with focus set on the top of the channels. Red area is represented

by image **(D)**. **D** Bright-field image of one cell container with loaded *H. Polymorpha* RB11 *MOX*-GFP cells. **E** SEM image of the microfluidic chip channel's cross-section with well bonding to a silanized glass cover slip. **F** SEM image of the microfluidic chip channel's cross-section without the glass cover slip (color figure online)

excitation at 410 nm, which could be attributed to the photoinitiator, but without having a negative effect on the detection of the cells. In vitro cytotoxicity test was performed according to ISO 10993-5 and indicated a high biocompatibility of the cured acrylate: relative cell viability was 109% (standard error of mean of =9%,  $n = 3$ ) compared to the control (see SI 1.1 for more details). From this point of view, the acrylate material was expected to not affect cell growth, e.g., due to leaching of toxic substances.

### 3.1.3 Rapid prototyping and optimization of cell container and cell loading

The centerpiece of the microfluidic chip for cell analysis was the container, i.e., the “dead end” part of a channel intersection (see Fig. 4). Container arrangement, length and angles were optimized iteratively, as modified chip designs could be tested out within short time periods due

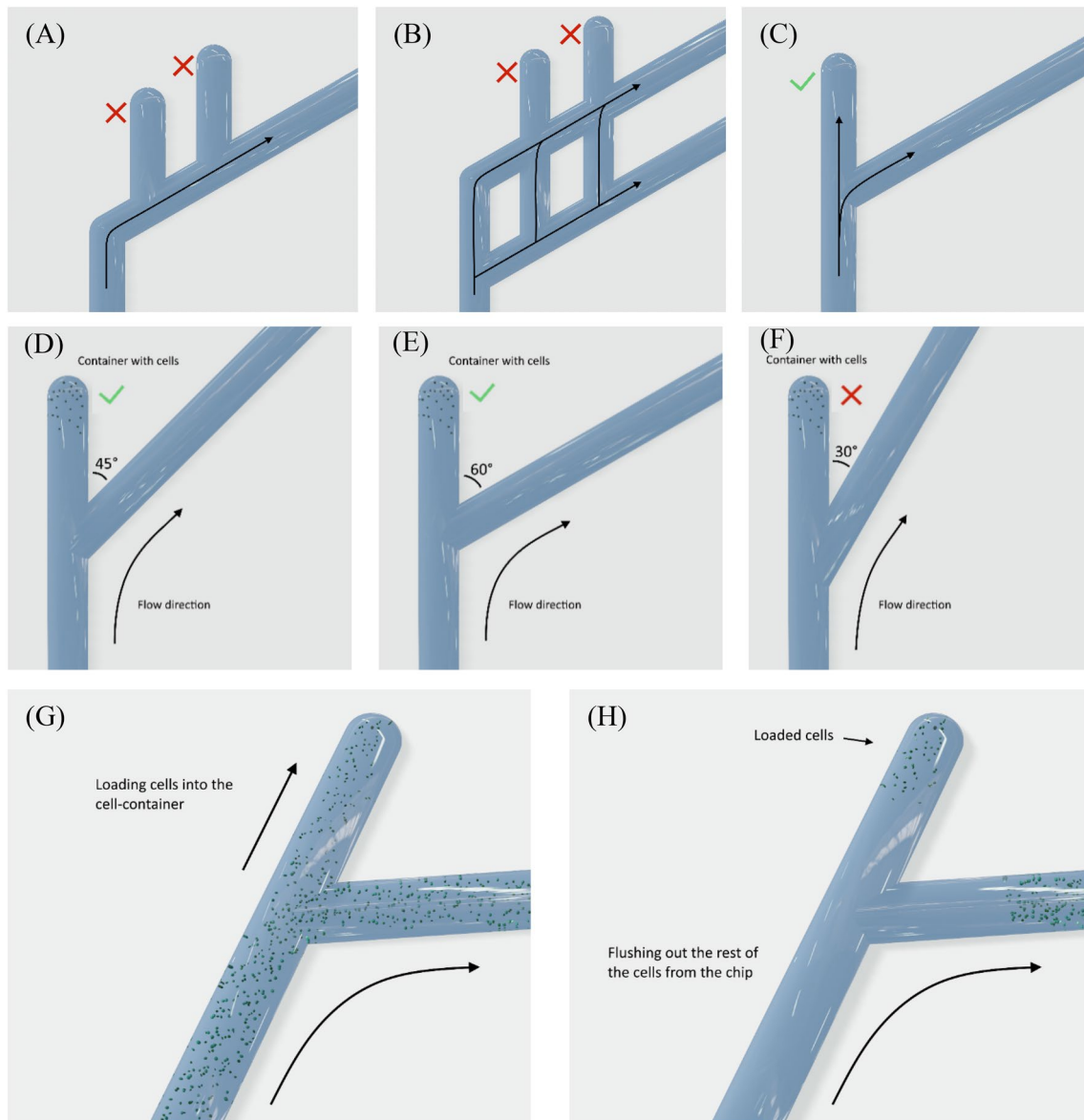


**Fig. 4** A–C Different types of cell containers. Black arrows show the direction of the flow. **A** The first design of the cell containers. **B** The second design of the cell containers. **C** The third final design. **D–F** Angles of 45°, 60° and 30° between the cell container and the channel towards the outlet, respectively. **G–H** Loading of the cells into the

microfluidic chip. **G** Manually loading the cells from the syringe with cell suspension into the cell container by increasing the pressure in the system. **H** Flushing out the rest of the cells from the chip with medium while loaded cells staying in the cell container

to the fast prototyping (Fig. 4A–F, see SI 1.4 for more details on the process). The cell container was approximately 300  $\mu\text{m}$  long, of which only the last 100  $\mu\text{m}$  were used to “catch” the cells for cultivation and analysis (Fig. 4G–H). The cells were loaded by combining cell inertia from acceleration in the channel right before the dead end and creating circular flow within the dead end by increasing pressure in the system. The loaded cells sedimented on the glass at the bottom of the cell container.

### 3.1.4 Medium exchange in the cell container

Because the cells in the cell container were not directly exposed to the liquid flow but were instead incubated in a 300  $\mu\text{m}$  long side cell container, it was essential to study the medium exchange. Since the fluorescence intensity is linearly correlated to the concentration of fluorescein, the medium exchange was analyzed by flushing the chip with 0.1 mM fluorescein and measuring the fluorescence intensity in the cell container. Figure 5 shows the fluorescence



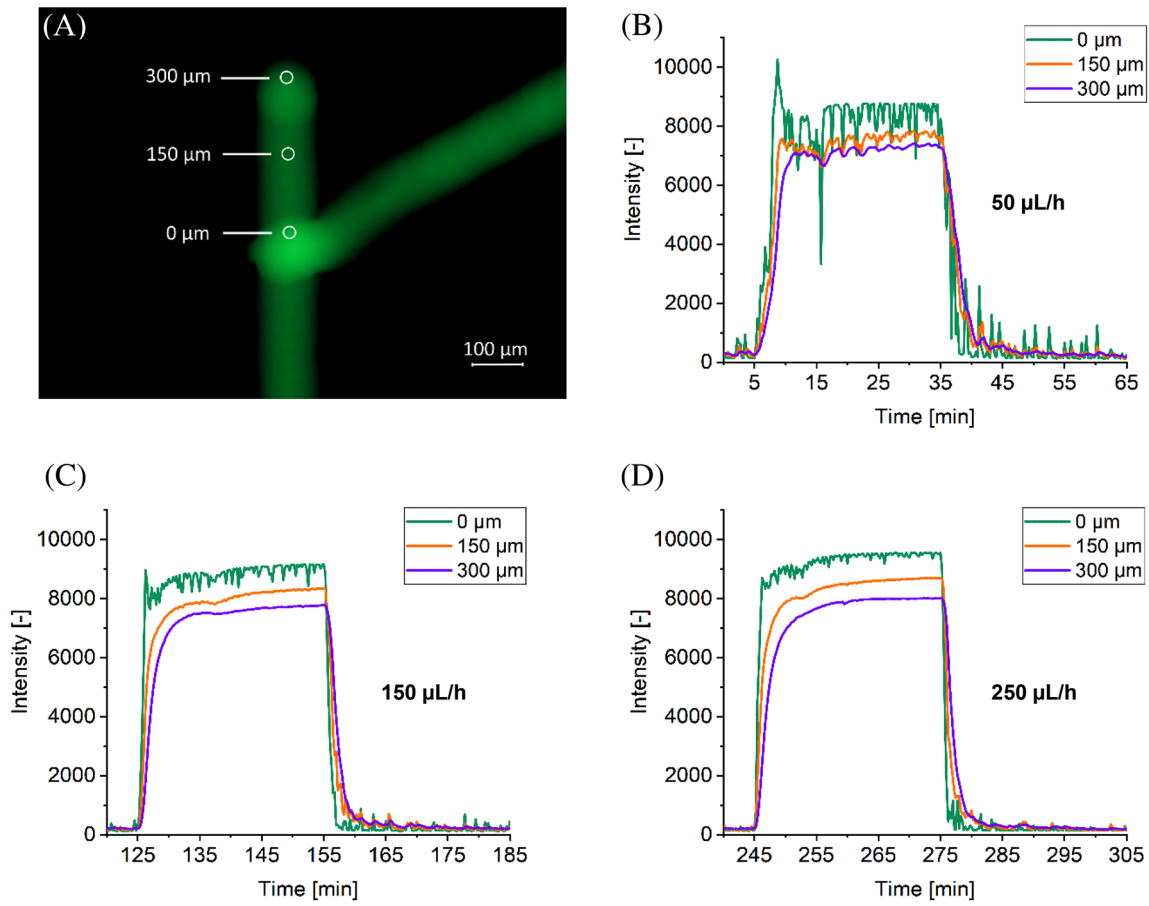


**Fig. 5** Medium exchange in the cell container. **A** Fluorescence image with marked points at 0 μm, 150 μm and 300 μm distance from the container inlet, at which measurements were taken. **B–D** The data collected at flow rates of 50 μL/h, 150 μL/h and 250 μL/h, respec-

tively. In all cases the medium was changed from water to fluorescein solution after 5.0 min and back to water after 35.0 min. The background fluorescence intensity was at least 100 units

intensities measured in the container at a distance of 0 μm, 150 μm and 300 μm from the container inlet at five different flow rates of 50, 100, 150, 200, and 250 μL/h.

With an integrated Y-piece, the dead volume of the system was approximately 0.035 μL and therefore negligible at any flow rate. When using an external Y-piece, the dead volume was approximately 2.5 μL, causing a delay of 3 min at the lowest flow rate of 50 μL/h. After the initial flushing with water at 50 μL/h, for each profile, the chip was flushed with fluorescein at the specific flow rate for 30 min, followed by flushing with water at the same rate for another 30 min. The data at a distance of 300 μm from the container inlet is of particular interest since the loaded cells were located there. Our results indicate that the maximum concentration, and hence full medium exchange, was achieved within 10 min after switching from water to 0.1 M fluorescein solution at all flow rates (see 5.0 min to 15.0 min in the graphs of Fig. 5). For the switching back from fluorescein solution to water, comparable switching rates were obtained. The differences in maximum fluorescence intensity between the

three detected positions could be attributed to differences in channel heights. The data also show that the fluorescein concentration at a distance of 300 μm from the container inlet was almost not affected by fluctuations in the rest of the system (represented by the point at 0 μm), which are especially noticeable at the lowest flow rate of 50 μL/h and are caused by the mechanics of the used low-pressure syringe pump system. In summary, the medium exchange in the cell container proved to be suitable for dynamic cell experiments described in the following section.

### 3.1.5 Functionalization of the cell container

During the silanization of the coverslips in preparation for the cryo-printing, the normally hydrophilic glass surface turned to hydrophobic. In contrast, *H. polymorpha* RB11 MOX-GFP cells did adhere to such hydrophobic glass surface very well (cf. Fig. 7), *C. glutamicum* DM1919 and *Synechocystis* sp. PCC 6803 proved to require hydrophilic surface characteristics for proper adhesion. For cultivation

experiments with these two cell types, the channel surface had to be re-functionalized. Two substances were tested as attachment promoters: poly(vinyl alcohol) and poly-L-lysine. Preparation with 1% poly(vinyl alcohol) solution resulted in a thin coating of poly(vinyl alcohol) which “peeled off” the channel walls and finally blocked the channels at the beginning of the experiments, deeming this method unusable. Re-functionalization with 0.04% poly-L-lysine solution, on the other hand, was effective – nearly 80% of loaded cells of both *C. glutamicum* DM1919 and *Synechocystis* sp. PCC 6803 were immobilized at the surface of the container, which enabled time-resolved experiments. However, the immobilization efficiency was decreasing along with chip usage time and chip age.

## 3.2 Cell cultivation experiments

The proposed microfluidic chip was tested with three physiologically different microorganisms—rod-shaped bacteria *C. glutamicum* DM1919, methylotrophic yeast *H. polymorpha* RB11 *MOX*-GFP, and unicellular phototrophic cyanobacteria *Synechocystis* sp. PCC 6803 to explore the range of cell applications that are possible with cryo-printed chips. All three microorganisms could be cultivated successfully for a few generations. Additionally, GFP production was induced in *H. Polymorpha* RB11 *MOX*-GFP by changing cultivation conditions, and the stability of GFP variant pHluorin2 was tested in *Synechocystis* sp. PCC 6803 pHluo in a separate experiment by varying the pH of the medium.

### 3.2.1 *Corynebacterium glutamicum* DM1919

In the first experiment, *Corynebacterium glutamicum* DM1919 cells were cultivated using chips that were re-functionalized with 0.04% poly-L-lysine solution as described above. The goal was to determine the applicability of chips for the cultivation of this type of bacteria. After loading the cells, it took approximately 15 min for the cells to sediment and adhere to the glass surface within the cell container (cf. Fig. 6B). The cells were cultivated under perfusion for over 6 h using fresh CGXII medium with glucose as a carbon source at a flow rate of 150  $\mu\text{L}/\text{h}$  and 23° C temperature. From the bright-field images taken every 30 min, several cells ( $n = 19$ ) were chosen and counted. It was observed that for the first 1.5 h, the cells increased in size without cell division (cf. Fig. 6D, E). If  $t = 1.5$  h was set as a starting point and  $t = 4$  h at which the number of cells doubled, a division rate of  $\nu = 0.28 \text{ h}^{-1}$  could be calculated. It is still lower than other reported cell division rates of  $\nu = 0.41 \text{ h}^{-1}$  to  $\nu = 0.79 \text{ h}^{-1}$  and cell growth rates of  $\mu = 0.37\text{--}0.65 \text{ h}^{-1}$  (Dusny et al. 2015; Grünberger et al. 2013). This can be explained as follows: (1) lower cultivation temperature (23° C in our case vs. 30° C in the sources), or (2) only those

cells which adhered well to the surface of the cell container throughout the entire time were counted, possibly leading to a biased characterization of a subculture not representing the entire cell sample. The experiment showed that it was possible to cultivate and quantitatively analyze the growth of *C. glutamicum* DM1919 on a single-cell level. Further tests need to be made either using poly-L-lysine of different molecular weights providing more attachment sites per unit square in the cell container, repeating the process of re-functionalization multiple times instead of one, or testing out other kinds of attachment factors. This could lead *C. glutamicum* DM1919 to grow in one layer during the whole duration of the experiment.

### 3.2.2 *Hansenula polymorpha* RB11 *MOX*-GFP

A dynamic experiment was carried out with *H. polymorpha* RB11 *MOX*-GFP by cultivating the cells at 23° C first for 4 h with SYN8 medium supplemented with 0.5% glucose (w/v) at 200  $\mu\text{L}/\text{h}$  and then switching to SYN8 medium without glucose for another 2.5 h to induce de-repression of *MOX*-promotor that controlled GFP synthesis. Its goal was to demonstrate the heterogeneity of *MOX*-promotor activity and determine the general ability to cultivate this cell type within the chip. The experiment was monitored by time-lapse microscopy at 30 min intervals with taking both bright-field and fluorescence images. The data for the cell-growth phase is shown in Fig. 7, while the GFP induction is depicted in Fig. 8. For the growth phase during the first 4 h, the growth rate of  $0.14 \text{ h}^{-1}$  was determined from the cell count, during which the number of cells nearly doubled (Fig. 7A). Specific growth rates of  $0.29 \text{ h}^{-1}$  and  $0.3 \text{ h}^{-1}$  were reported from cultivating the same type of cells in shake flasks within SYN8 medium at 30° C (Dusny and Schmid 2016). However, the cultivation in their case was carried out at 30° C, and the data was taken from the exponential growth phase, whereas the first 4 h indicate a similar curve slope, which is in close correspondence to the cultivation data using our microfluidic chip. Thus, it could be stated that it was possible to maintain the conditions present in the shake flasks using the proposed microfluidic chip, while also observing the cells on the single-cell level with a continuous medium exchange in the cell container. After the growth phase, the medium was switched to SYN8 medium without glucose at the flow rate of 200  $\mu\text{L}/\text{h}$ . According to the previously described results of the medium-exchange experiment, the set-up was left for 10 min to enable the medium exchange in the cell container before starting the time-lapse microscopy monitoring. The results show that the onset of GFP synthesis in *H. polymorpha* RB11 *MOX*-GFP cells already begins only 30 min after the medium change (Fig. 8A), which agrees with reported GFP maturation times reported

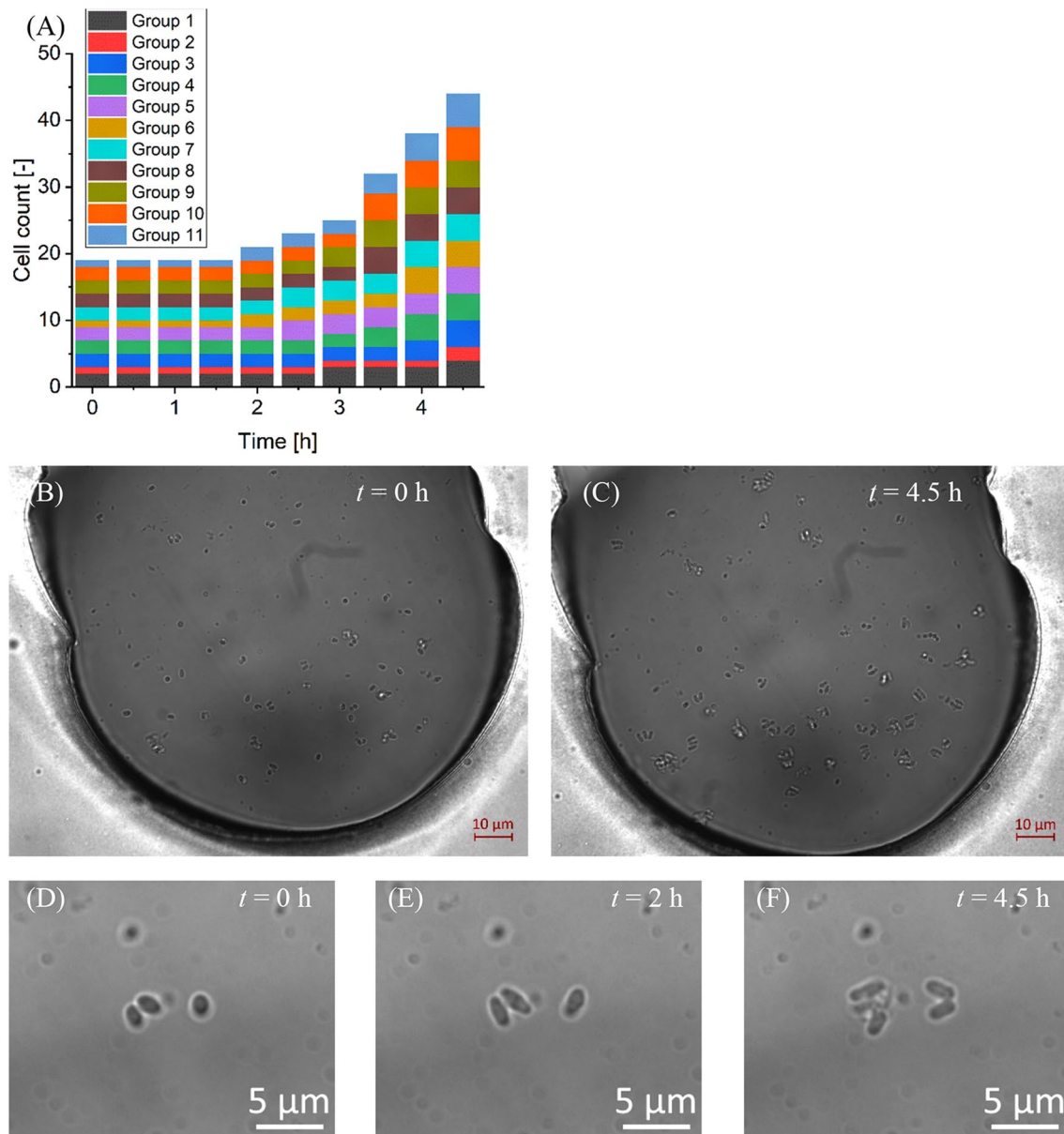


**Fig. 6** Cultivation of *C. glutamicum* DM1919. **A** Growth of picked 19 cells over the first 4.5 h of the experiment. **B** The cell container at the beginning of the experiment after the cells sedimented on the bottom

of the cell container,  $t = 0$  h. **C** The cell container towards the end of the experiment, at  $t = 4.5$  h. **D–F** An excerpt from a cell container at  $t = 0$ ,  $t = 2$  h and  $t = 4.5$  h, respectively.

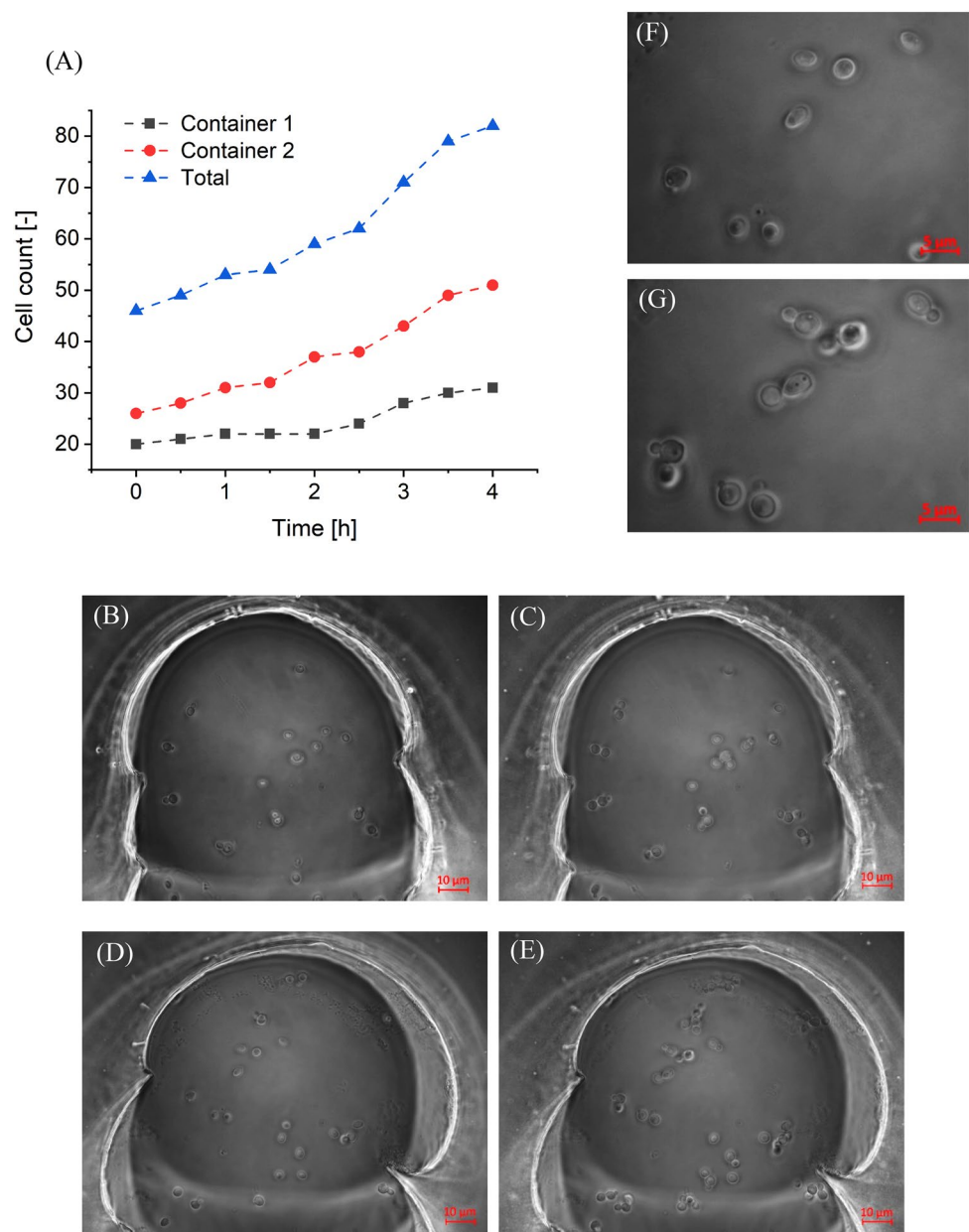
(Chalfie et al. 1994; Cubitt et al. 1995). The maximum intensity of cell fluorescence due to GFP synthesis was reached at approximately 1.5 h. After that time, GFP intensity began to decrease due to the depletion of glucose as carbon and energy source. Nearly identical results were reported from experiments using an alternative single-cell based cultivation system with *H. polymorpha* RB11 MOX-GFP being trapped directly in the flow of SYN8 medium without any glucose (Dusny and Schmid 2016). Phenotypic heterogeneity in GFP synthesis increased along with

GFP intensity, reached its maximum, and tapered off after two hours of incubation (Fig. 8A, B).

### 3.2.3 *Synechocystis* sp. PCC 6803

The last series of experiments were run with *Synechocystis* sp. PCC 6803 with a three-fold purpose: to examine the chip's suitability for bio-applications with phototrophic types of microorganisms, test the stability of GFP protein, and demonstrate its heterogeneity. The hydrophobicity of

**Fig. 7** *H. Polymorpha* RB11 MOX-GFP growth experiment. **A** Graph showing the growth of *H. Polymorpha* RB11 MOX-GFP in two cell containers. **B–E** Bright-field images of cell containers with loaded *H. Polymorpha* RB11 MOX-GFP cells corresponding to the graph. **B** Container 1,  $t=0$  h. **C** Container 1,  $t=4$  h. **D** Container 2,  $t=0$  h. **E** Container 2,  $t=4$  h. **F–G** Cutouts from bright-field images **D** and **E**, respectively



the cell surface was similar to *C. glutamicum* DM1919, and the chips, therefore, had to be re-functionalized with 0.04% poly-L-lysine solution to carry out the experiments. In the first experiment, the cells were cultivated in YBG11 medium over 24 h at a light intensity of  $75 \mu\text{E m}^{-2} \text{s}^{-1}$  (Fig. 9). 2–3 cell divisions with a specific growth rate of  $0.05 \text{ h}^{-1}$  were observed. In the second set of experiments, the performance of a fluorescent ratiometric GFP-based pH-sensor pHluorin2 (Mahon 2011) was tested by alternating the pH of the PBS medium in the chip. The pH was repeatedly changed from  $\text{pH}=6$  to  $\text{pH}=9$  in 30-min intervals for 6 h as an example of another dynamic application with this microfluidic chip. The results show high stability of pHluorin2 throughout the entire experiment in that

similar fluorescence intensity ratios are observed through repeated pH change cycles (Fig. 10A). This is even though below  $\text{pH}=5.5$  and above  $\text{pH}=8.5$ , the protein stops responding to changes in pH, suggesting decreased stability outside the pH range of 5.5–8.5 (Maresová et al. 2010; Reifenrath and Boles 2018). It can also be observed that there is a more significant variance between 488 to 410 nm intensity ratios at  $\text{pH}=6$  than at  $\text{pH}=9$ , with mean sample standard deviation being  $\bar{s} = 0.02$  and  $\bar{s} = 0.08$  respectively (Fig. 10A, C). The reason for this tendency is that the cells exhibit greater heterogeneity when excited at 488 nm and  $\text{pH}=6$  when compared to  $\text{pH}=9$ , while the excitation at 410 nm results in similar heterogeneity at both pH values (Fig. 10B).

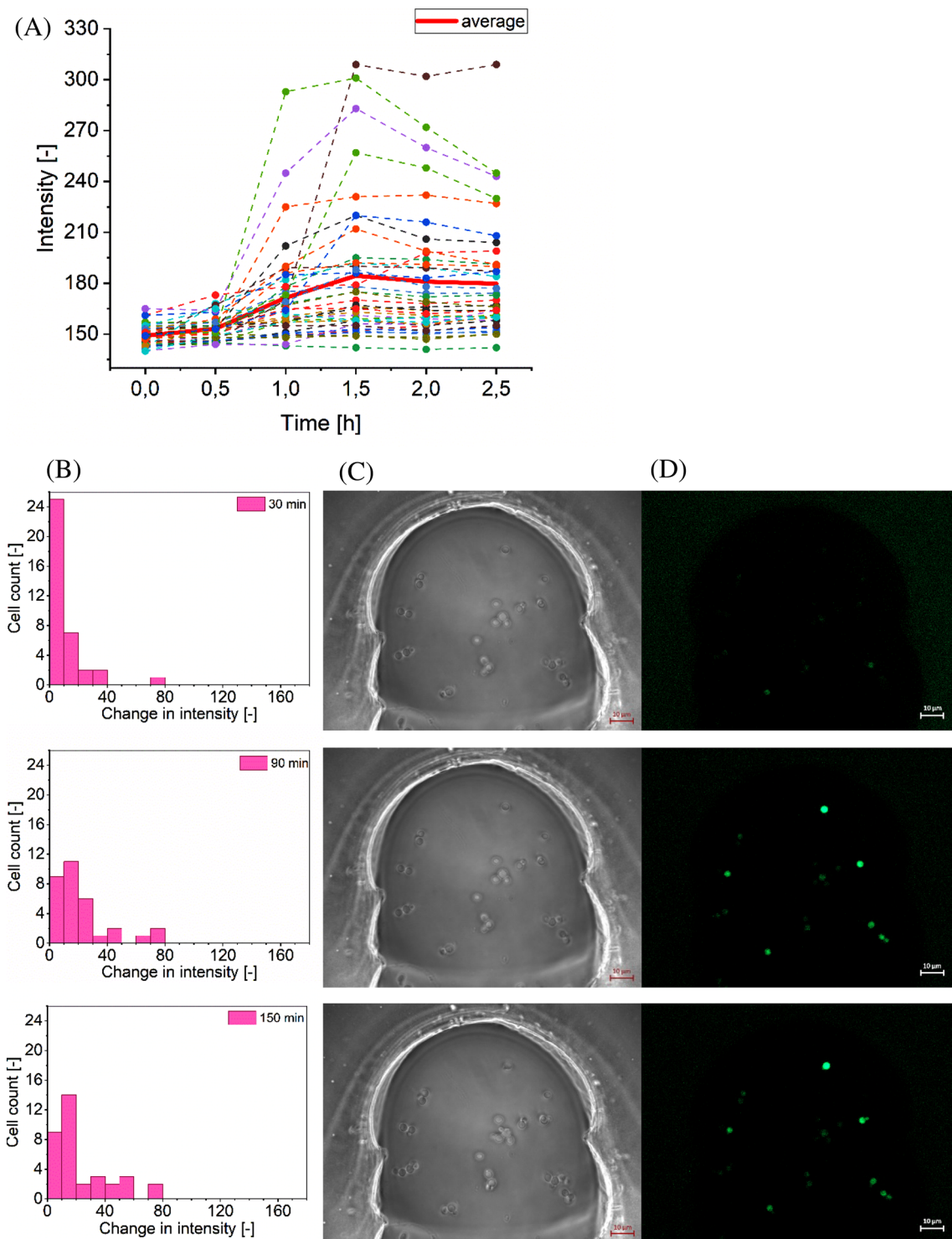
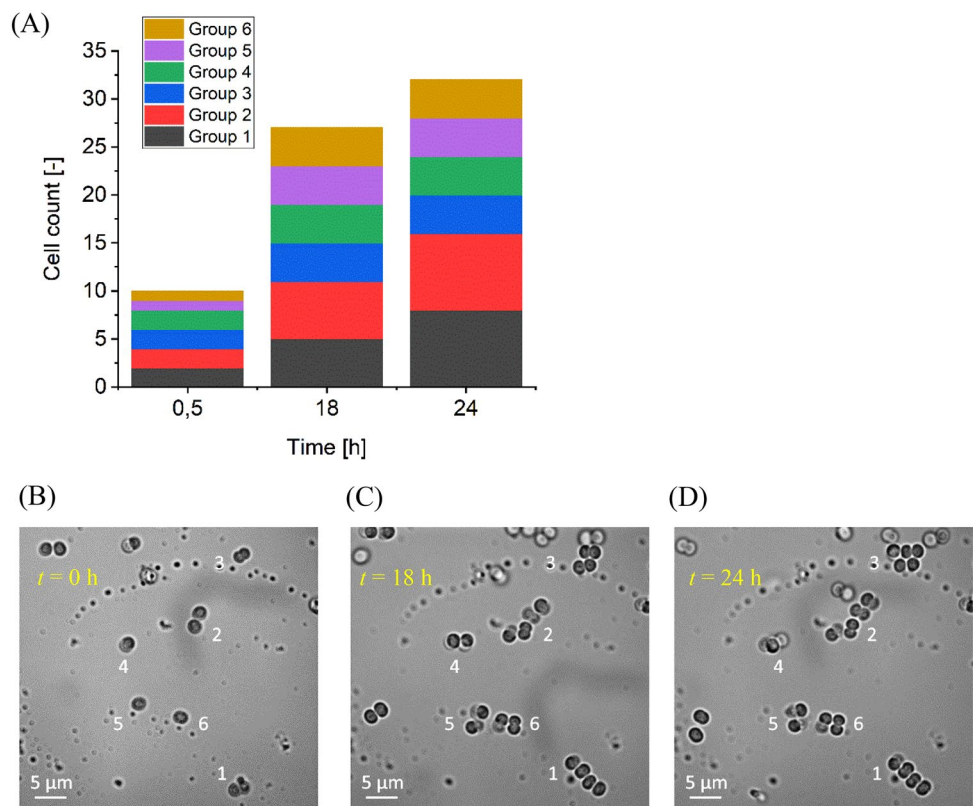


**Fig. 8** Single-cell MOX-promotor activity in *H. Polymorpha* RB11 MOX-GFP. **A** GFP fluorescence intensities over the first 2.5 h. The intensity at  $t=0$  h is reference GFP fluorescence intensity before changing the medium without glucose to medium with glucose. Data taken from two cell chambers, with total analyzed cell number  $n=37$ . **B** The distribution of GFP fluorescence intensities at  $t=0.5$  h,

$t=1.5$  h and  $t=2.5$  h, respectively. Data corresponding to the previous graph (A). **C** Bright-field images of one of the two cell chambers with *H. polymorpha* RB11 MOX-GFP at  $t=0.5$  h,  $t=1.5$  h and  $t=2.5$  h, respectively. **D** Corresponding fluorescence images of *H. Polymorpha* RB11 MOX-GFP

**Fig. 9** The cultivation of *Synechocystis* sp. PCC 6803 WT. **A** The graph shows the growth of *Synechocystis* sp. PCC 6803 WT over the period of 24 h. **B–D** The bright-field images correspond to the time points in the graph of 0 h, 18 h and 24 h, respectively. The numbers in the images correspond to the group numbers in the graph



## 4 Conclusion and outlook

This work demonstrates the cryo-printing technology as a new method to rapidly fabricate microfluidic chips for cell analysis. Although the development required many minor modifications to the initial design of the chip, multiple iterations were possible thanks to the rapid prototyping nature of the method and the low cost per chip. As a result, a microfluidic chip with specially designed containers for analyzing three types of morphologically different cell types was developed. *C. glutamicum* DM1919, *H. Polymorpha* RB11 MOX-GFP, and *Synechocystis* sp. PCC 6803 were successfully loaded into a cell container and cultivated. Additionally, GFP production was induced and measured in *H. Polymorpha* RB11 MOX-GFP by depleting the glucose in the cell container to the minimum required concentration to de-repress the MOX-promotor. Additionally, the stability of GFP variant pHluorin2 was tested out with *Synechocystis* sp. PCC 6803 pHluo over multiple cycles of switching between buffers of different pH and measuring pHluorin2 response. In all experiments, various degrees of heterogeneity between cells were observable, showing the microfluidic chip's capability for cell analysis at single-cell resolution. The experiments were possible due to quick medium exchange in the cell container, which was explicitly tested beforehand. In summary, the

cryo-printing technology proved to be applicable in this field of research, although it is certainly not limited to it.

However, additional work is necessary to optimize the produced chips for cell analysis. The re-functionalization of the silanized glass surface needs to be optimized, allowing for an even higher number of cell generations per experiment to be analyzed. Modification to channel surface's smoothness during the printing process could be realized by increasing the temperature slightly before curing the acrylic layer with UV-LED.

The cryo-printing technology offers many possibilities due to its high flexibility and adaptability. Microfluidic structures can be printed on different substrates, enabling a facile integration of different functionalities, e.g., electrodes. We successfully tested a variety of substrates in preliminary studies—polymer slides, foils, silicon wafers, and metals. Additionally, functionalities can be generated in-situ during the printing process by changing from water to solutions containing biomolecules or polymerizable monomers. In this way, for example, porous structures can be integrated within the channels acting as filter or membrane or biomolecule-functionalized reactors. Even more advanced applications can be achieved using multiple micro-dispenser nozzles of different diameters or with different solutions. Finally, the cryo-printing process can be easily upscaled and automatized, which offers, despite the rapid prototyping, a great potential for small-batch

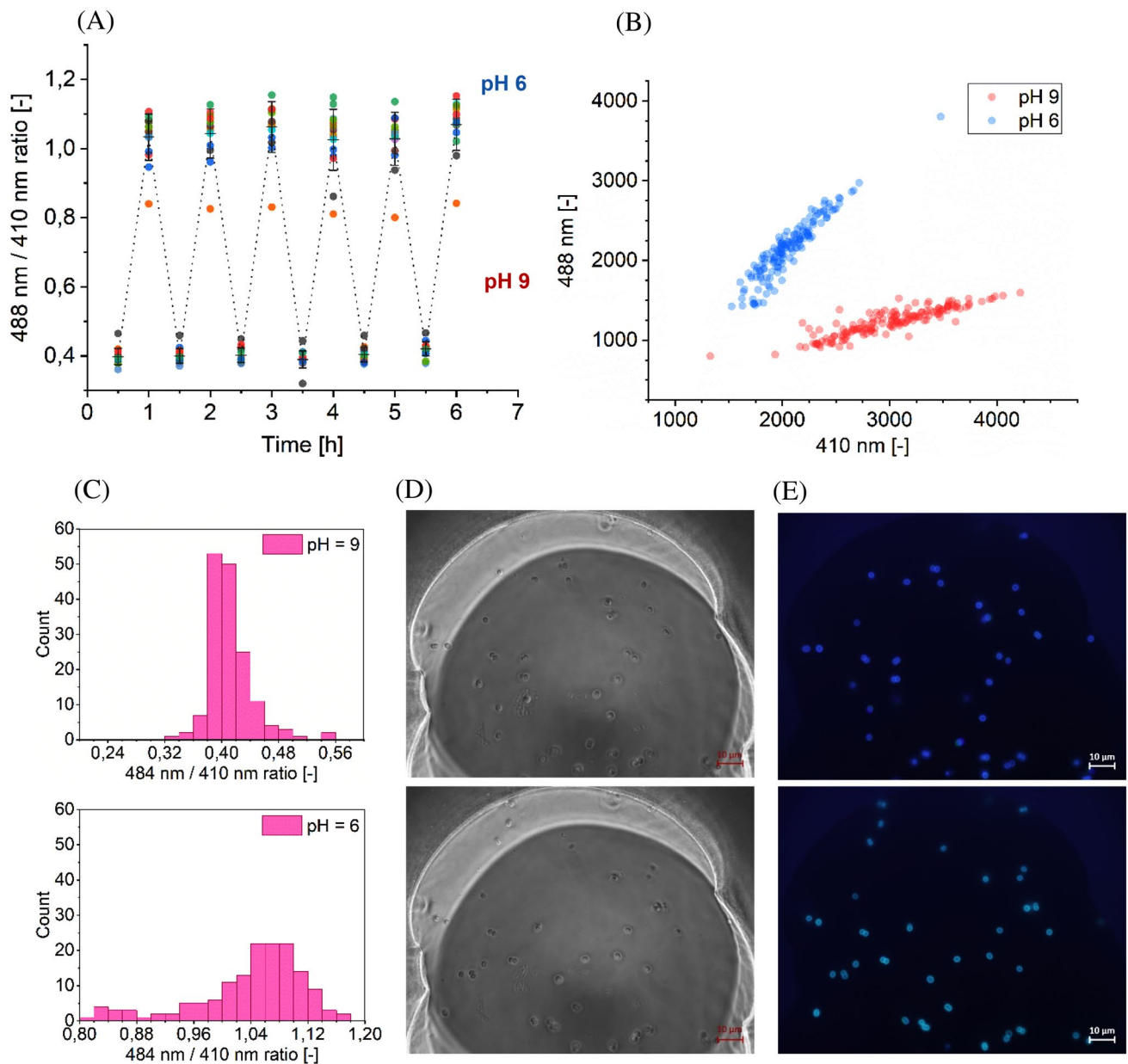


**Fig. 10** *Synechocystis* sp. PCC 6803 pHluo. **A** The 488 nm to 410 nm ratio of chosen  $n=16$  cells at alternating pH=9 and pH=6. **B** Distribution of fluorescence intensities at different pH with number of cells at both pH=6 and pH=9 being at least  $n=150$ . **C** Distribution of fluorescence intensity ratios at pH=9,  $t=0.5$  h and pH=6,

$t=1$  h. Total number of analyzed cells  $n=16$ . **D** Bright-field images of the cell chamber with *Synechocystis* sp. PCC 6803 pHluo. **E** Corresponding fluorescence images of the cell chamber with *Synechocystis* sp. PCC 6803 pHluo

production and could be interesting for small-cap companies, e.g., in the field of microfluidic disposables.

**Acknowledgements** The authors thank Kristin Lindstaedt (UFZ) for cultivating the cells and support during cell experiments. Furthermore, the authors want to acknowledge Christoph Nolte for his help in developing the acrylate cover layer material. Special thanks goes to Franziska Zitzmann (Robitzki group, Centre for Biotechnology and Biomedicine BBZ) for performing the in vitro cytotoxicity assay. Finally,

the authors want to thank Andrea Prager (IOM) for taking the SEM images in Fig. 3E and F.

**Author contributions** Concept and design of experiments: CD, CH, RG; experimental performance: RG, CH; cryoprinter—idea and concept: CE; setup: CE, AC, RG, CH; visualization: RG; writing—original draft preparation: RG, CH; writing—editing: RG, CH, CD; supervision and project administration: AS, BA. All authors reviewed and commented on the manuscript.

**Funding** Open Access funding enabled and organized by Projekt DEAL.

## Declarations

**Conflict of interest** The authors declare that they have no conflict of interest.

**Open Access** This article is licensed under a Creative Commons Attribution 4.0 International License, which permits use, sharing, adaptation, distribution and reproduction in any medium or format, as long as you give appropriate credit to the original author(s) and the source, provide a link to the Creative Commons licence, and indicate if changes were made. The images or other third party material in this article are included in the article's Creative Commons licence, unless indicated otherwise in a credit line to the material. If material is not included in the article's Creative Commons licence and your intended use is not permitted by statutory regulation or exceeds the permitted use, you will need to obtain permission directly from the copyright holder. To view a copy of this licence, visit <http://creativecommons.org/licenses/by/4.0/>.

## References

- Amin R, Knowlton S, Hart A, Yenilmez B, Ghaderinezhad F, Katebifar S, Messina M, Khademhosseini A, Tasoglu S (2016) 3D-printed microfluidic devices. *Biofabrication* 8:22001. <https://doi.org/10.1088/1758-5090/8/2/022001>
- Au AK, Huynh W, Horowitz LF, Folch A (2016) 3D-printed microfluidics. *Angew Chem Int Ed Engl* 55:3862–3881. <https://doi.org/10.1002/anie.201504382>
- Beebe DJ, Mensing GA, Walker GM (2002) Physics and applications of microfluidics in biology. *Annu Rev Biomed Eng* 4:261–286. <https://doi.org/10.1146/annurev.bioeng.4.112601.125916>
- Chalfie M, Tu Y, Euskirchen G, Ward WW, Prasher DC (1994) Green fluorescent protein as a marker for gene expression. *Science* 263:802–805. <https://doi.org/10.1126/science.8303295>
- Cubitt AB, Heim R, Adams SR, Boyd AE, Gross LA, Tsien RY (1995) Understanding, improving and using green fluorescent proteins. *Trends Biochem Sci* 20:448–455. [https://doi.org/10.1016/S0968-0004\(00\)89099-4](https://doi.org/10.1016/S0968-0004(00)89099-4)
- Dusny C, Schmid A (2015) Microfluidic single-cell analysis links boundary environments and individual microbial phenotypes. *Environ Microbiol* 17:1839–1856. <https://doi.org/10.1111/1462-2920.12667>
- Dusny C, Schmid A (2016) The MOX promoter in *Hansenula polymorpha* is ultrasensitive to glucose-mediated carbon catabolite repression. *FEMS Yeast Res*. <https://doi.org/10.1093/femsyr/fow067>
- Dusny C, Grünberger A, Probst C, Wiechert W, Kohlheyer D, Schmid A (2015) Technical bias of microcultivation environments on single-cell physiology. *Lab Chip* 15:1822–1834. <https://doi.org/10.1039/c4lc01270d>
- Grünberger A, van Ooyen J, Paczia N, Rohe P, Schiendzielorz G, Eggeling L, Wiechert W, Kohlheyer D, Noack S (2013) Beyond growth rate 0.6: *Corynebacterium glutamicum* cultivated in highly diluted environments. *Biotechnol Bioeng* 110:220–228. <https://doi.org/10.1002/bit.24616>
- Ho CMB, Ng SH, Li KHH, Yoon Y-J (2015) 3D printed microfluidics for biological applications. *Lab Chip* 15:3627–3637. <https://doi.org/10.1039/c5lc00685f>
- Jiang J, Zhan J, Yue W, Yang M, Yi C, Li C-W (2015) A single low-cost microfabrication approach for polymethylmethacrylate, polystyrene, polycarbonate and polysulfone based microdevices. *RSC Adv* 5:36036–36043. <https://doi.org/10.1039/C5RA02220G>
- Kelly BE, Bhattacharya I, Heidari H, Shusteff M, Spadaccini CM, Taylor HK (2019) Volumetric additive manufacturing via tomographic reconstruction. *Science* 363:1075–1079. <https://doi.org/10.1126/science.aau7114>
- Levis M, Kumar N, Apakian E, Moreno C, Hernandez U, Olivares A, Ontiveros F, Zartman JJ (2019) Microfluidics on the fly: inexpensive rapid fabrication of thermally laminated microfluidic devices for live imaging and multimodal perturbations of multicellular systems. *Biomicrofluidics* 13:24111. <https://doi.org/10.1063/1.5086671>
- Mahon MJ (2011) pHluorin2: an enhanced, ratiometric, pH-sensitive green fluorescent protein. *Adv Biosci Biotechnol* 2:132–137. <https://doi.org/10.4236/abb.2011.23021>
- Maresová L, Hosková B, Urbánková E, Chaloupka R, Sychrová H (2010) New applications of pHluorin—measuring intracellular pH of prototrophic yeasts and determining changes in the buffering capacity of strains with affected potassium homeostasis. *Yeast* 27:317–325. <https://doi.org/10.1002/yea.1755>
- Morgan AJL, Hidalgo San Jose L, Jamieson WD, Wymant JM, Song B, Stephens P, Barrow DA, Castell OK (2016) Simple and versatile 3D printed microfluidics using fused filament fabrication. *PLoS ONE* 11:e0152023. <https://doi.org/10.1371/journal.pone.0152023>
- Nielsen AV, Beauchamp MJ, Nordin GP, Woolley AT (2020) 3D printed microfluidics. *Annu Rev Anal Chem (palo Alto Calif)* 13:45–65. <https://doi.org/10.1146/annurev-anchem-091619-102649>
- Reidy TM, Luo D, Rana P, Huegel B, Cheng X (2019) Transparency of PDMS based microfluidic devices under temperature gradients. *J Micromech Microeng* 29:15014. <https://doi.org/10.1088/1361-6439/aaf028>
- Reifenrath M, Boles E (2018) A superfolder variant of pH-sensitive pHluorin for in vivo pH measurements in the endoplasmic reticulum. *Sci Rep* 8:11985. <https://doi.org/10.1038/s41598-018-30367-z>
- Rosenthal K, Falke F, Frick O, Dusny C, Schmid A (2015) An inert continuous microreactor for the isolation and analysis of a single microbial cell. *Micromachines* 6:1836–1855. <https://doi.org/10.3390/mi6121459>
- Sackmann EK, Fulton AL, Beebe DJ (2014) The present and future role of microfluidics in biomedical research. *Nature* 507:181. <https://doi.org/10.1038/nature13118>
- Shallan AI, Smejkal P, Corban M, Guijt RM, Breadmore MC (2014) Cost-effective three-dimensional printing of visibly transparent microchips within minutes. *Anal Chem* 86:3124–3130. <https://doi.org/10.1021/ac4041857>
- Stankova NE, Atanasov PA, Nikov R, Nikov RG, Nedyalkov NN, Stoyanov TR, Fukata N, Kolev KN, Valova EI, Georgieva JS, Armyanov S (2016) Optical properties of polydimethylsiloxane (PDMS) during nanosecond laser processing. *Appl Surf Sci* 374:96–103. <https://doi.org/10.1016/j.apsusc.2015.10.016>
- Sun X, Peeni BA, Yang W, Becerril HA, Woolley AT (2007) Rapid prototyping of poly(methyl methacrylate) microfluidic systems using solvent imprinting and bonding. *J Chromatogr A* 1162:162–166. <https://doi.org/10.1016/j.chroma.2007.04.002>
- Tumbleston JR, Shirvanyants D, Ermoshkin N, Januszewicz R, Johnson AR, Kelly D, Chen K, Pinschmidt R, Rolland JP, Ermoshkin A, Samulski ET, DeSimone JM (2015) Additive manufacturing. Continuous liquid interface production of 3D objects. *Science* 347:1349–1352. <https://doi.org/10.1126/science.aaa2397>
- Waheed S, Cabot JM, Macdonald NP, Lewis T, Guijt RM, Paull B, Breadmore MC (2016) 3D printed microfluidic devices: enablers and barriers. *Lab Chip* 16:1993–2013. <https://doi.org/10.1039/c6lc00284f>
- Zhang H, Li H, Wu M, Yu H, Wang W, Li Z (2014) 3D ICE printing as a fabrication technology of microfluidics with pre-sealed reagents. In: Ayazi F (ed) IEEE 27th International Conference on



- Micro Electro Mechanical Systems (MEMS), 2014: 26–30 Jan. 2014, San Francisco, CA, USA. IEEE, Piscataway, NJ, pp 52–55
- Zhang H, Zhang F, Huang D, Zhou Y, Zhang X, Li Z (2015) Microcapsule array fabricated by ice-printing technology for on-site biochemical detection. In: 2015 Transducers—015 18th International Conference on Solid-State Sensors, Actuators and Microsystems (TRANSDUCERS). IEEE, pp 757–760
- Zheng F, Pu Z, He E, Huang J, Yu B, Li D, Li Z (2018) From functional structure to packaging: full-printing fabrication of a microfluidic chip. *Lab Chip* 18:1859–1866. <https://doi.org/10.1039/c8lc00327k>

**Publisher's Note** Springer Nature remains neutral with regard to jurisdictional claims in published maps and institutional affiliations.